Journal of Computational Applied Mechanics 2021, 52(4): 619-641
DOI: 10.22059/jcamech.2021.330072.648

RESEARCH PAPER

Implementation of Behavior-Based Navigation Algorithm on Four-Wheel Steering Mobile Robot

Behzad Saeedi, Majid Sadedel*

[a] *Mechatronics Laboratory, Department of Mechanical Engineering, Tarbiat Modares University, Tehran, Iran*

Abstract

In recent years, wheeled autonomous mobile robots have become widely used in a number of industrial applications. Therefore, accurate and efficient controllers are required in order to assure safe and accurate navigation of these vehicles. In this study, an effective behavior-based navigation algorithm (BBNA) is applied to control the trajectory of the four-wheel steering (FWS) mobile robot. The BBNA combines the 'Goal-to-Goal' and 'Obstacle Avoidance' behaviors into one comprehensive navigation strategy. With this algorithm, many switching between modes occurs over a short amount of time, which increases the risk of creating the chattering phenomenon. Due to overcoming this phenomenon, an additional mode is considered between the 'Go-to-Goal' and 'Obstacle Avoidance' modes that is called 'Follow-Wall' behavior. At first, the BBNA was designed to control the navigation of a point mass robot. One of the significant characteristics of BBNA is that its control commands can be used to calculate the linear and angular velocity of a unicycle mobile robot. Thus, the BBNA can navigate the unicycle mobile robot successfully to the goal position. In order to apply the BBNA to an FWS mobile robot, its dynamic equations must be converted to those of a unicycle mobile robot. The present study determines the dynamic equations of the FWS mobile robot by using the Ackermann- Jeantnat model of steering. Since these equations are the same as those for the unicycle mobile robot, the FWS mobile robot can be controlled by the BBNA. Finally, the implementation of the BBNA for the FWS mobile robot is simulated using MATLAB software. Simulated results indicate that BBNA generates an optimal path by perfectly switching between 'Go to Goal', 'Obstacle Avoidance', and 'Follow Wall' modes, which keeps the FWS mobile robot arriving at the goal position.

Keywords:

Four-Wheel Steering Mobile Robot, Navigation Algorithm, Unicycle Mobile Robot, Behavior-Based Control.

1. Introduction

1.1. State of the Art

Mobile robots are of the newly-appearing technologies in the field of transportation such that this technology, owing to the simple and reliable structures, can change people's lifestyles, travel, and work in cities[1, 2]. Another feature of mobile robots is to be "autonomous" meaning that the robot can move around in their environment without human intervention[3]. Mobile robots fall into several major categories, including legged robots[4–6], wheeled robots[7] and tracked robots[8]. Legged robots cross uneven terrain, whereas wheeled and tracking robots have fine efficiency over smooth and continuous lands. There are several classes of wheeled robots, for instance, autonomous vehicles that each wheel can steerable independently, mobile robots with two steering wheels so that their orientation mechanism is similar to a car, and omnidirectional autonomous

* Corresponding author. Email Address: majid.sadedel@modares.ac.ir
Tel.: +98 21 82884987; fax: +98 21 82884987.

mobile robots[9, 10]. In an omnidirectional mobile robots, none of the wheels change their direction, but these robots can supply excellent mobility which leads to efficient movement in various environments[11]. Another important class of wheeled robots is an FWS mobile robot that each wheel is activated by a separate hub motor. This category of autonomous mobile robots can achieve motion in an arbitrary direction because each wheel can be steerable independently of the other wheels. FWS mobile robots are widely employed in rough land, space exploration, automated factories, disaster save, etc [12–15].

Recently, due to the importance of mobile robots, significant effort has been made by researchers to control the movement of mobile robots[16–18]. Various researches have been done to receive a satisfactory output tracking of mobile robots. Based on energy consumption and dynamic vehicle behavior, Valera and et al[19], found an optimal method for the navigation of autonomous mobile robots. The successful performance of this method is confirmed by the actual tests of a lightweight vehicle under different situations that include different obstacles positions and dynamic parameters. Through the use of sliding mode tracking control,Lee and et al[20] found the control inputs for the indicated arbitrary paths of a mobile robot With the Lyapunov stability theory, they showed that position tracking error approaches zero asymptotically. In their study, the performance of the controller designed has been proved through computer simulations. A linear-quadratic regulator (LQR) controller for trajectory control is presented in Fnadi and et al.'s study of an off-road autonomous vehicle[21]. They demonstrated that the LQR controller method has high accuracy for routes that follow by high and low-speed. Carlucho and et al[22] used reinforcement learning algorithms to offer a new expert controller for mobile robots. They showed the high efficiency of the proposed controller of mobile robots under various conditions. Wang and et al [23] presented an optimal path-following control method based on robust model predictive control for an omnidirectional autonomous mobile robot in real-world conditions. Allaghui and et al[24], developed a highly effective control strategy using the (PID) controller concept. They employed this strategy to navigation of the autonomous robot Khepera II. The results of these researchers demonstrated the proper performance and efficiency of the suggested methodology. Maalouf and et al[25], presented a fuzzy inference system to overcome the problem of the sideslip of the autonomous mobile robot. In regard to the system output constraints, Hu and et al[26] adopted a different approach of output constraint controller to strengthen the stability of the system. For an FWS autonomous mobile robot,Wang and Qi[27] developed an algorithm for trajectory planning based on vehicle robot kinematics. Caracciolo and et al [28] provided a robust controller for navigation control of an autonomous car-like robot. Filpescu and et al[29] improved the tracking ability of FWS mobile robots by using the dynamic model of the car-like vehicles.

The development of autonomous vehicles that robustly operate in populated areas and provide several services to humans is the main purpose of researchers in the field of mobile robots. Therefore, the use of various control systems is needed to make mobile robots successfully ‘Go-to-Goal', ‘Obstacle Avoidance’ and ‘Follow a Wall’. A behavior-based control strategy is a promising method that includes different controllers in order to the motion control of mobile robots in dynamic and various environments[30, 31]. In this method, by designing an integrated structure, it is very simpler to control the trajectory of mobile robots. One of the essential features of this control method is that it allows us to add new modes to the control algorithm without causing significant complexity in its control structure. For this purpose, Egerstedt[32–34] presented a full navigation system so that this architecture includes ‘go-to-goal’, ‘Obstacle Avoidance’, and ‘Follow-Wall’ behaviors. In other to examine the efficiency of this navigation system, Egerstedt[35] implemented this control algorithm on a Nomad 200 mobile robot and verified its

performance. Khazaee and et al[36] used the navigation algorithm to control the motion of the Hexapod robot. Their simulation tests show that the proposed navigation approach with appropriate switching between different behaviors has been very efficient in generating an optimal trajectory for the Hexapod mobile robot. Also, Amrah and et al[37], presented effective navigation architecture. Using a MATLAB robot simulator, they implemented this navigation algorithm and demonstrated that this algorithm is very effective in achieving various goals such as 'move to a goal point', 'follow a line', and 'obstacle avoidances'.

1.2. Contribution

Based on studies conducted by the authors of this paper, it appears that there are very few studies that have completed a complete navigation algorithm for a four wheel steering mobile robot. As a four wheel steering mobile robot has four independent wheels, each of which can be controlled independently and which can change the steering angle, they are used in a variety of industries like service robots or navigation in difficult terrain. Consequently, in the navigation of these robots, it is essential to use an algorithm that incorporates a complete navigation architecture that guides the robot to the objective through an optimized path without encountering obstacles. The BBNA controller is a behavior-based control algorithm that provides complete control over the navigation and guidance of a point mass model robot with high accuracy and quality. This algorithm contains 'Go-to-Goal', 'Follow-Wall', and 'Obstacle Avoidance' modes such that the robot selects an appropriate behavior according to its position and the location of the goal and obstacles. In the mentioned algorithm, hard switches are used to change the control modes. Furthermore, a boundary following behavior which is called sliding dynamics is considered between 'Go-to-Goal' and 'Obstacle Avoidance' modes to overcome the chattering phenomena and also enable the robot to bypass the boundary around the obstacles. As mentioned above, A BBNA is based on generating an optimal path for a point mass robot. An easy trick can be used to convert the control commands generated for a point mass model robot into linear and angular velocity commands for a unicycle mobile robot. The purpose of this research is to apply BBNA algorithms to complete navigation of FWS mobile robots. To accomplish this, Ackermann-Jeantnat's method will be applied so that FWS' equations of motion are identical to those of unicycle mobile robots. The BBNA algorithm will then be applied to the FWS mobile robot.

Consequently, the main contribution of this research can be summarized as follows:

- ✓ Using Ackermann-Jeantnat's method, equations of FWS mobile robot are extracted similarly to equations of unicycle mobile robot. Due to the FWS mobile robot's four independent wheels, each of which has the ability to change the steering angle independently, the method allows us to calculate the speed of the internal and external wheels by using the linear velocity and angular velocity of the robot structure.
- ✓ FWS mobile robot navigation is achieved by the BBNA complete navigation controller, which includes behaviors such as 'Go-to-Goal', 'Follow Wall', and 'Obstacle Avoidance'. It is noted that by implementing Ackermann-Jeantnat's method for extracting FWS mobile robot equations similar to those of the unicycle mobile robot, it is possible to implement BBNA for navigation of the FWS mobile robot.

Finally, a variety of simulation experiments are used to analyze the performance and efficiency of the control algorithm for FWS mobile robot navigation. Additionally, the steering angles of the inside and outside wheels of lean (the width-to-length ratio of the robot is less than one) and fat (the width-to-length ratio of the robot is greater than one) FWS mobile robots are examined.

1.3. Outline

The rest of this paper is set as follows: In section 2 the kinematic model of the FWS mobile robot has been introduced by using the Ackermann-Jeantnat model of steering. The BBNA has been explained in section 3. In section 4, by using MATLAB software, simulations of the system and controller performance are provided. Concluding and comments are put forward in section 5.

2. Mathematical Modeling and Formulation

2.1. Preliminaries

Ackermann-Jeantnat steering geometry model is a geometric configuration of linkages in the steering of a car or other vehicle when the vehicle is running at low speed[38–40]. The purpose of the Ackermann geometry model is a static analysis of vehicle steering by ignoring the centrifugal force and the effect of tires' side slips[41]. According to this model, which is shown in Fig. 1, the steering angle of the robot is done with the help of two front wheels (δ_{in} and δ_{out}) and the two rear wheels of the robot are responsible to move the robot. Moreover, $2L$ represents the distance between the front and back wheels, and $2W$ represents the distance between the two rear wheels.

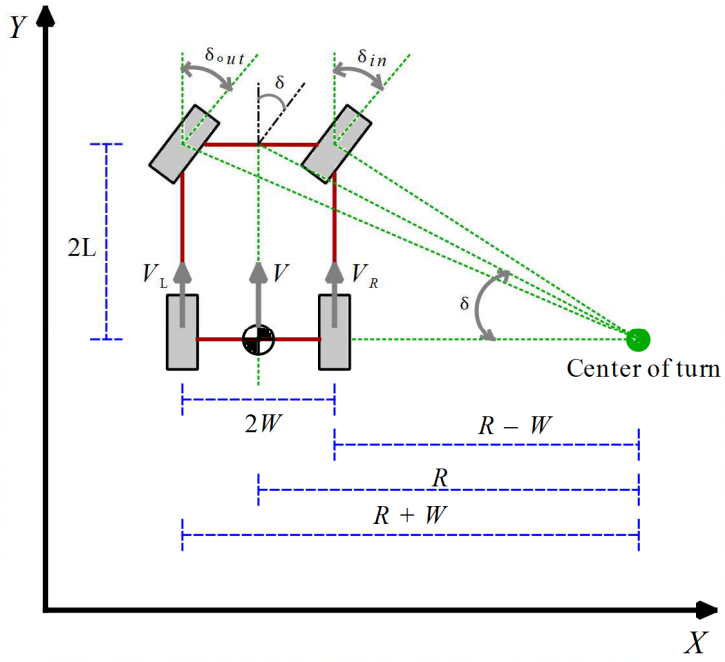

Figure 1. Ackermann-Jeantad steering geometry model

The basic purpose of the Ackermann-Jeantnat model is to calculate the speed of the two rear wheels during steering and rotation radius R as the following:

$$V_R = V - \left(\frac{W}{R} \times V\right) \tag{1}$$

$$V_L = V + \left(\frac{W}{R} \times V\right) \tag{2}$$

Where V is the vehicular velocity and rotation radius can be obtained as:

$$R = \frac{2L}{\tan(\delta)} \tag{3}$$

Where δ is defined as the Ackermann-Jeantnat angle[41]. By assuming small angles in the turn, the steer angles can be calculated as:

$$\delta_{in} = \frac{2L}{R - W} \tag{4}$$

$$\delta_{out} = \frac{2L}{R + W} \tag{5}$$

Therefore, the Ackermann-Jeantnat geometry model can be used to explain the kinematic geometrical relationship of internal and external wheels when steering an autonomous vehicle.

2.2. Description and Kinematics of the FWS Mobile Robot

A scheme of FWS mobile robot is depicted in Fig. 2. Each wheel of the FWS mobile robot has an individual steering motor, so there are four independent wheels. As shown in Fig. 2, (X_G, Y_G) is a primary inertia frame and (X_R, Y_R) is another coordinate that has been fixed on the mobile robot. Furthermore, θ demonstrates the diversion angle between the robot and the primary inertia frame. Also, in this figure, $2L$ and $2W$ demonstrates the length and width of the robot respectively.

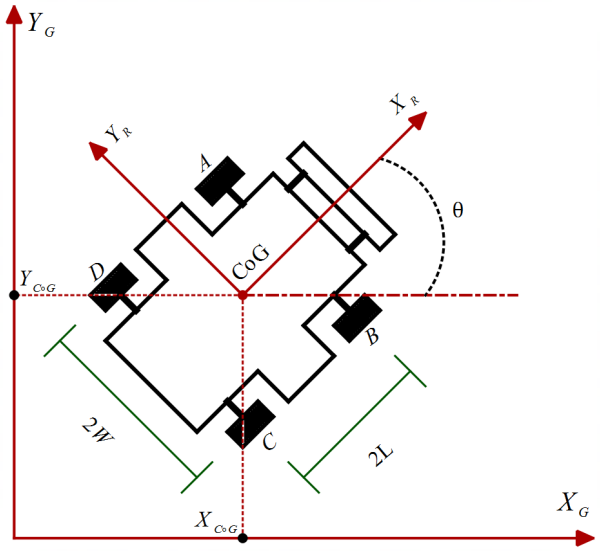

Figure 2. The scheme of an FWS mobile robot.

As shown in Fig. 2 the origin of the mobile robot is considered the center of gravity (CoG). The robot wheels have the following positions at their centers:

$$\begin{cases} x_A = X_{CoG} + h\cos(\alpha + \theta) \\ y_A = Y_{CoG} + h\sin(\alpha + \theta) \end{cases} \tag{6}$$

$$\begin{cases} x_B = X_{CoG} + h\cos(-\alpha + \theta) \\ y_B = Y_{CoG} + h\sin(-\alpha + \theta) \end{cases} \tag{7}$$

$$\begin{cases} x_C = X_{CoG} + h\cos(\pi + \alpha + \theta) \\ y_C = Y_{CoG} + h\sin(\pi + \alpha + \theta) \end{cases} \tag{8}$$

$$\begin{cases} x_D = X_{CoG} + h\cos(\pi - \alpha + \theta) \\ y_D = Y_{CoG} + h\sin(\pi - \alpha + \theta) \end{cases} \tag{9}$$

Where:

$$h = \sqrt{L^2 + W^2}, \quad \alpha = \tan^{-1}\left(\frac{W}{L}\right) \tag{10}$$

In the above equations, (X_{CoG}, Y_{CoG}) shows the position of the robot CoG and the center of the robot wheels are illustrated by A, B, C, and D.

For mathematical modeling of the system, the following nonholonomic constraints are considered[42]:

a) The intervals between all the wheels are constant.

b) The lateral slip is ignored.

c) There are no flexible elements on the FWS mobile robot.

The nonholonomic constraint of robot CoG determinate is considered:

$$\dot{X}_{CoG}\sin(\theta) + \dot{Y}_{CoG}\cos(\theta) = 0 \tag{11}$$

The nonholonomic constraints for each wheel can be obtained. For example, in equation (12) the nonholonomic constraint for wheel is presented.

$$\dot{x}_A\sin(\theta + \gamma) + \dot{y}_A\cos(\theta + \gamma) = 0 \tag{12}$$

In the above equation, γ illustrate the angle between the wheel and X_R direction.

As shown in Fig. 3, there is an equal linear velocity for the two inside wheels and an equal linear velocity for the two outside wheels. This condition can be used to simplify the mathematical model.

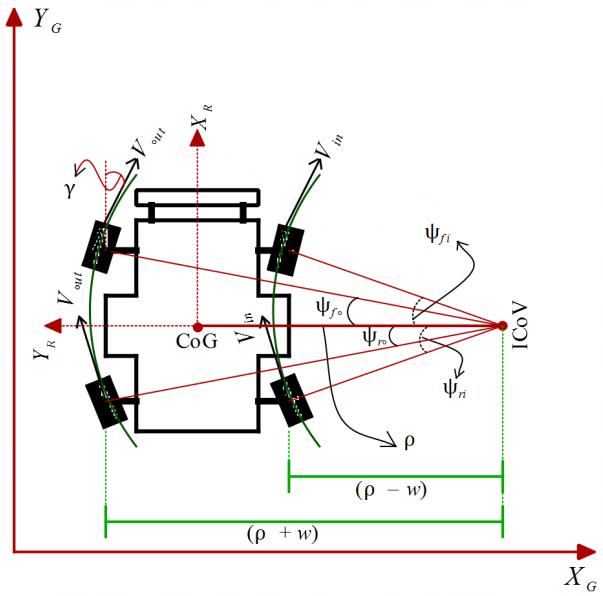

Figure 3. A model of front and rear differential steering of FWS mobile robot.

According to Fig. 3, when the FWS autonomous robot is rotating, the axis line of each wheel points to the robot instantaneous center of velocity (ICoV), therefore, the angular velocity of each wheel around the ICoV is equal. Furthermore, the distance between the CoG and the ICoV is ρ and $\psi_{fi}, \psi_{fo}, \psi_{ri}, \psi_{ro}$ are the steering of the inside front wheel, the outside front wheel, the inside rear wheel and the outside front wheel respectively. As depicted in Fig. 3, the steering angle of all wheels can be obtained as follows:

$$\cot(\psi_{fi}) = \cot(\psi_{ri}) = \frac{\rho - W}{L} \tag{13}$$

$$\cot(\psi_{fo}) = \cot(\psi_{ro}) = \frac{\rho + W}{L} \tag{14}$$

According to these equations, when a robot travels on a curved trajectory, the steering angle of the inner wheels is equal, so the outer wheels are also subject to this property. Consequently, the outer and inner wheels have the following relationship:

$$\cot(\psi_{fo}) - \cot(\psi_{fi}) = \frac{2W}{L} \tag{15}$$

For the rear wheel, it can be concluded that:

$$\cot(\psi_{ro}) - \cot(\psi_{ri}) = \frac{2W}{L} \tag{16}$$

Since that the mobile robot is running at low speed, for mathematical modeling of the FWS autonomous robot we can use the Ackermann-Jeantnat [43] model of steering. According to this model, the ICoV is located along a midline that divides the length of the robot into two equal parts. So, the radius of curvature can be determined as follows:

$$\rho = \frac{L}{\tan(\theta)} \tag{17}$$

Furthermore, the linear velocity of the inside and outside wheels can be described as follows:

$$v_{in} = \frac{\rho_{in} v}{L} \tan(\theta) \tag{18}$$

$$v_{out} = \frac{\rho_{out} v}{L} \tan(\theta) \tag{19}$$

Where $v$is vehicle velocity in the X_R direction, and:

$$\rho_{in} = \sqrt{(\rho - w)^2 + (L)^2} \tag{20}$$

$$\rho_{out} = \sqrt{(\rho + w)^2 + (L)^2} \tag{21}$$

Finally, by determining the linear and angular velocity of the CoG of the FWS mobile robot, the dynamic equations of the system in the global coordinate system are calculated as follows:

$$\begin{cases} \dot{x} = v \times \cos(\theta) \\ \dot{y} = v \times \sin(\theta) \\ \dot{\theta} = \omega \end{cases} \tag{22}$$

Therefore, we convert the complex dynamic equations of the FWS mobile robot into motion equations of a simple robot with two inputs $[v, \omega]$ which the above equations are the same as the dynamic equations of the unicycle mobile robot.

2.3. The Validation of the FWS Mobile Robot's Equations

It is one of the major capabilities of a four-wheeled steering mobile robot that it can actively steer its rear wheels during turning maneuvers, so verification and validation of the steering angles of each wheel is necessary in this study. Assume that the front wheels are solely responsible for controlling the robot's movement and that the rear wheels are straight at the steering angle. In this case, Fig. 4 illustrates that the center of velocity instantaneously will be in the direction of the axis of rotation of the rear wheels, as a result of the linear velocity of the front and rear wheels. This is exactly how Figure 1 illustrates that Ackermann-Jeantnat's theory will work correctly when analyzing system behavior.

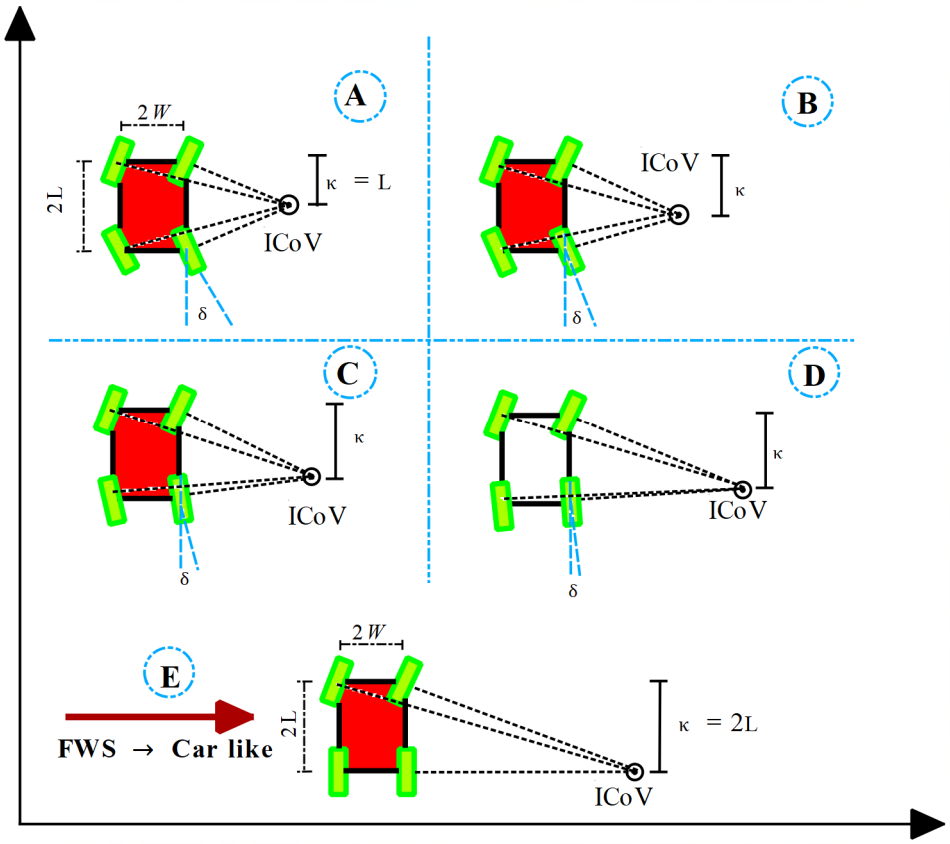

Figure 4. Effects of steering the rear wheels on the instantaneous center of velocity

As a result of the extraction of the internal and external wheels velocity of the FWS mobile robot with the help of the instantaneous center of velocity, the validity of the equations extracted with the help of the Ackerman theory is established. Fig. 5 shows the geometry of the turn of a FWS vehicle. Thomas[41] calculated the physical behavior of the vehicle as well as the steering angles of each wheel, the instantaneous center of velocity, and its radius. In this figure, $\zeta, T_d, \lambda, \mathrm{d_c}, d, r, R, \delta_f, \delta_r, L$ are angle between the drive shaft and the horizontal axis, torque, angle between the steer axis and the vertical direction, distance from the center of the wheel to the beginning of the drive shaft, the distance between the wheel center and the steering axis on earth, radius of wheel, radius of instantaneous center of velocity, front steering angle, rear steering angle, and length of the vehicle, respectively.

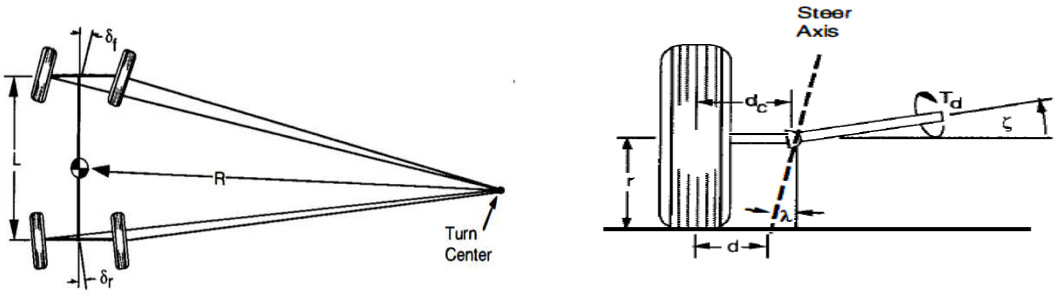

Figure 5. A schematic showing the geometry of a FWS vehicle turn[41]

According to Tomas'[41] kinematic analysis of the vehicle, the radius of the instantaneous center of velocity can be calculated as follows:

$$R = \frac{L}{\delta_f(1+\zeta)} \tag{23}$$

Due to the fact that the axis of the robot drive shaft presented in this study does not change its angle with respect to the horizon, as a result, the ζ value becomes zero in equation (23), giving the same result as we have presented in equation (17). As shown in Fig. 4, the position and radius of the instantaneous center of velocity change as the steering angle of the rear wheels of the robot decreases. By reducing the amount of δ from state A to E, the instantaneous center of velocity is closer to the axis of the rear wheels of the robot, so that in position E, the instantaneous center of velocity is exactly in line with the rear wheels. Ackermann-Jeantnat's theory for a car-like mobile robot is exactly the same as case E. As a confirmation of what has been described above, and to investigate the effect of the position of the instantaneous center of velocity on the steering angle of the front wheels of the robot and also the radius of the instantaneous center of velocity, Fig. 6 is presented. In this figure, κ shows the distance between the center of velocity and the front of the robot. In Fig. 6, items (a) and (b) illustrate the effect of changing the instantaneous center of velocity's position (κ) and radius (R) on the steering angle of the inner and outer wheels on the front axle of the robot ($\delta_{in}, \delta_{out}$). As shown in the diagram, at a certain position of the instantaneous center of the velocity (i.e.$\kappa = 75$), the steering angle of the wheels ($\delta_{in}, \delta_{out}$) decreases with

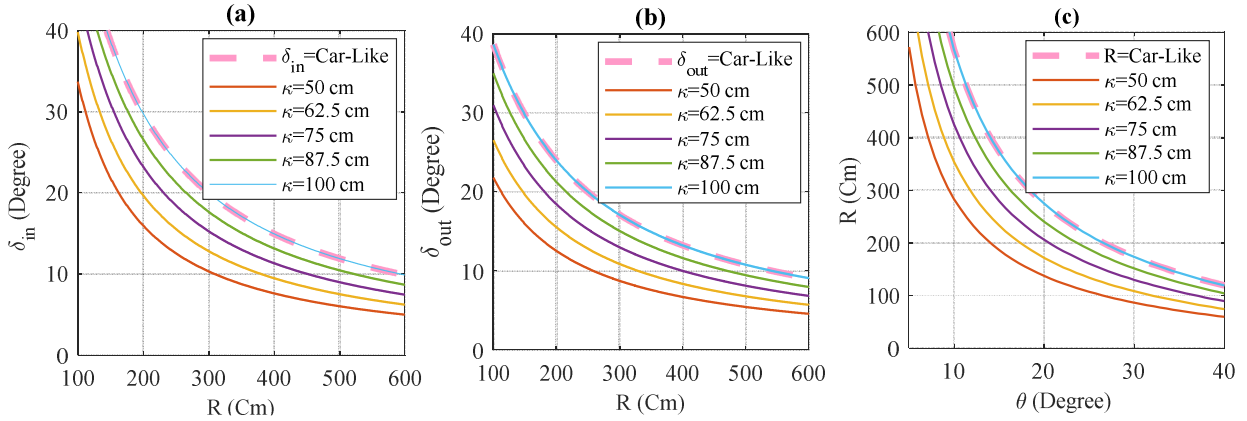

Figure 6. a & b) The influence of changing the instantaneous center of velocity on the steering angle of the inner and outer wheels in front of the robot, **c)** The effect of steering angle and instantaneous center of velocity position on the instantaneous center of velocity radius

increasing the radius of the instantaneous center (R). On the other hand, by changing κ and increasing it, the diagram of changes in the steering angle at (a) and (b) is placed on a car-like diagram, which its model was presented by Ackermann-Jeantnat.

Likewise, case (c) in Fig. 6 shows that increasing the robot steering angle reduces the radius of the instantaneous center of velocity (R) for a given κ. The diagram shows that as κ increases (decreases in δ for FWS robot shown in Fig. 4), the two diagrams are closer together, so that at $\delta = 0$, they are exactly matched, which confirms the accuracy of the equations for the FWS mobile robot.

3. Control Algorithms

As stated before, several different control modes are necessary to control autonomous mobile robot navigation, and all of these types together create a control structure known as a BBNA. Accordingly, this section shows how the two main behaviors of “goal attraction” and “obstacle

avoidance" are presented in a BBNA. As demonstrated in Fig. 7, the BBNA consists of Go-to-Goal (GTG), Follow-Wall (FW), and Obstacle Avoidance (OA) behaviors[33, 35]. So that when the robot meets the obstacle, depending on the position of the goal, the robot will follow the wall around the obstacle clockwise or counterclockwise.

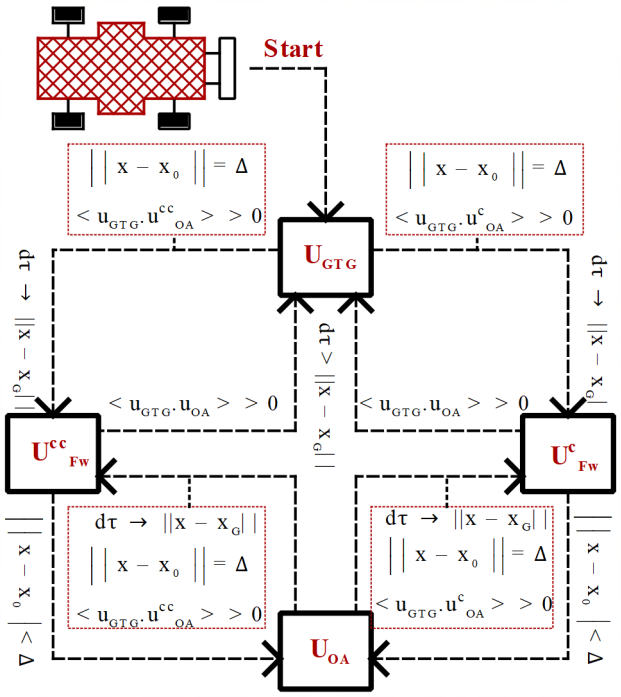

Figure 7. Setup for navigation algorithm.

A BBNA is based to control the trajectory tracking of a point mass robot so that with two transformations, this method can be used to control a FWS mobile robot. A point mass robot has the following equation of motion:

$$\dot{X} = \begin{bmatrix} u_x \\ u_y \end{bmatrix}, \quad \left(X = \begin{bmatrix} x \\ y \end{bmatrix} \in \Re^2 \right) \tag{24}$$

In this equation, X represents the motion vector in the global coordinate system.

3.1. Go-To-Goal (GTG)

Using $X_{Goal} = (x_{Goal}, y_{Goal})$ as the location of the goal point in the global coordinates, the following error function can be defined:

$$e_{GTG} = X_{Goal} - X \tag{25}$$

Where the robot's position in global coordinates is defined by X. The control input for point mass robot can be defined as bellows:

$$u_{GTG} = K(\|e_{GTG}\|)e_{GTG} \tag{26}$$

The derivative of equation (25) is:

$$\dot{e}_{GTG} = -K(\|e_{GTG}\|)e_{GTG} \tag{27}$$

According to equation (26), when the robot is too far from the goal point, the proposed controller may apply high input to the robot actuators, in which case the possibility of saturation in the actuators increases. To solve this problem, one solution is to write $K(\|e_{GTG}\|)$ as a function of error e_{GTG} as bellow:

$$K(\|e_{GTG}\|) = \frac{a\left(1 - e^{-b\|e_{GTG}\|^2}\right)}{\|e_{GTG}\|} \tag{28}$$

Where a and b are positive constant. As shown in equation (28), the system is asymptotically stable if $K(\|e_{GTG}\|)$ is positive definite.

3.2. Obstacle Avoidance (OA)

The sensors are used in mobile robots to detect the position of obstacles ($X_o = (x_o, y_o)$) in the global coordinate system. The sensors form a circular area with a safe radius of (d_0) around the center of mass of the mobile robot. Therefore, obstacles that are close to this safe area are detected by the mobile robot. In this case, the error function is:

$$e_{OA} = X_O - X \tag{29}$$

The control input for obstacle avoidance of the point mass robot would be designed as follows:

$$u_{AO} = K(\|e_{OA}\|)e_{OA} \tag{30}$$

Although the GTG behavior of the BBNA shall be so designed to ensure that the response of the system is stable, the controller of the OA behavior needs to produce an unstable motion. The reason for using the unstable controller in OA behavior is to prevent the robot from hitting the obstacle. To reach this proposed manner, K_{AO} can be written as:

$$K(\|e_{OA}\|) = -\frac{c}{\|e_{OA}\|(\|e_{OA}\|^2 + \varepsilon)} \tag{31}$$

Where c and ε are positive constants that are used to tuning the controller.

3.3. Follow Wall (FW)

As shown in Fig. 8, a suitable approach to motion control of the robot to reach the goal position is to use hard switches between GTG and OA behaviors. Near the position of the obstacles, a large number of switches between GTG and OA behaviors may occur in a short period of time with this hybrid system for controlling the movement of the mobile robot. This phenomenon is the so-called Zeno, which can increase the chattering in the controller strategy. Furthermore, in pure OA behavior, the robot drives away from the obstacle and moves in the other path, which this strategy is too conservative.

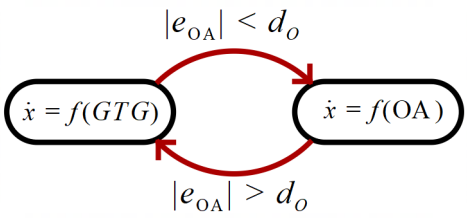

Figure 8. The hard switches between the GTG and OA behaviors

To overcome the stated cases of the hybrid system, one would define a new behavior in an automaton, which is demonstrated in Fig. 9. The added node in this figure containing the sliding dynamics that are presented on the switching surface between the GTG and OA modes. As shown in Fig. 10, the additional mode is the "boundary following" behavior so that the robot should be able to move around the safety area surrounding an obstacle.

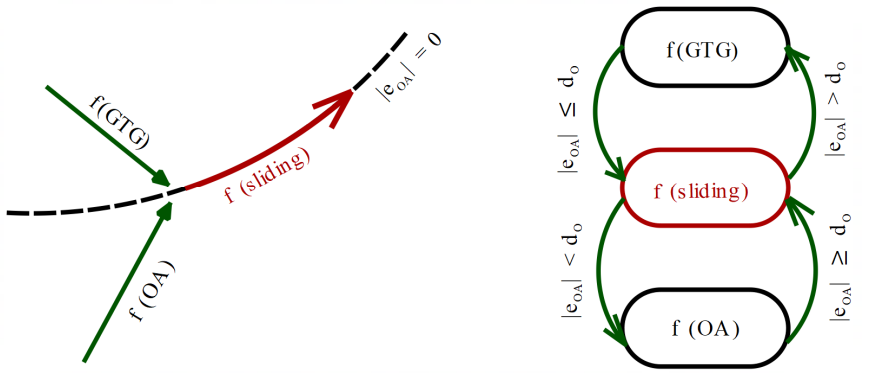

Figure 9. Regularization of a Zeno phenomenon

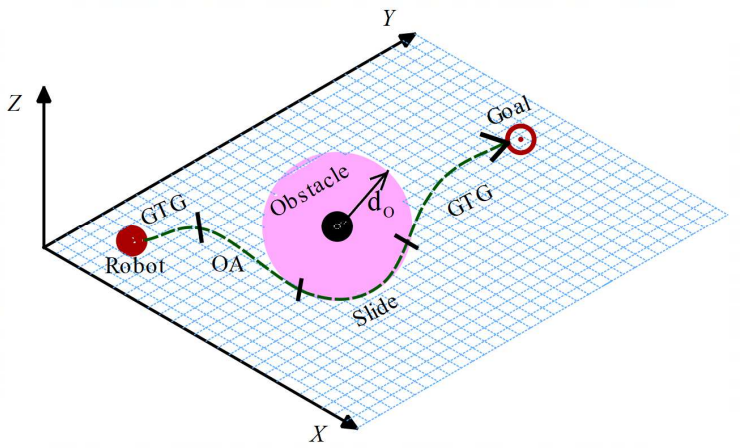

Figure 10. Goal attraction together with obstacle avoidance by considering sliding dynamic

Therefore, the wheeled robots can move along the boundary of the obstacle in clockwise (C) and counterclockwise (CC) directions. For this purpose, by rotating u_{AO} through $\pi\backslash 2$ and $-\pi\backslash 2$, the control input needed to follow the boundary of the obstacle in C and CC directions can be obtained as follows:

$$u_{FW}^{CC} = \mu R\left(\frac{\pi}{2}\right) u_{OA} \tag{32}$$

$$u_{FW}^{C} = \mu R\left(-\frac{\pi}{2}\right) u_{OA} \tag{33}$$

In the above equation, μ is a constant that is used to obtain a suitable induced mode. Moreover, $R(\varphi)$ represents the rotation matrix that can be derived by equation (34):

$$R(\varphi) = \begin{bmatrix} \cos\varphi & -\sin\varphi \\ \sin\varphi & \cos\varphi \end{bmatrix} \tag{34}$$

Furthermore, in order to follow the boundary of the obstacle, robot needs an appropriate direction that can be obtained by using the dot product of u_{GTG} and u_{FW}. The appropriate direction for different conditions are presented in equation (35) and (36).

$$if \rightarrow \langle u_{GTG}, u_{FW}^{cc} \rangle > 0 \Longrightarrow u_{FW}^{cc} \tag{35}$$

$$if \rightarrow \langle u_{GTG}, u_{FW}^{c} \rangle > 0 \Longrightarrow u_{FW}^{c} \tag{36}$$

Also, another issue that needs to be addressed is when the robot stops following the boundary of an obstacle and switch back to the goal attraction behavior. As shown in equations (32)-(33), this time is when "enough progress" has been achieved and the robot has "clear shot" toward the goal position.

$$\|X - X_{Goal}\| < \|X(\tau) - X_{Goal}\| \Rightarrow ENOUGH\ \ POGRESS \tag{37}$$

$$\langle u_{OA}, u_{GTG} \rangle > 0 \Longrightarrow CLEAR\ SHOT \tag{38}$$

Where τ represent the time of the last switch. The initial condition in equation (37) shows that the robot is nearer the goal position than it was in the initial moment of following the boundary around the obstacle. The second condition stated in equation (38) is established when the directions of the velocity vectors in the GTG and the OA behaviors are compatible. With the help of these two conditions, the mobile robot will move towards the goal position through an optimal path.

The BBNA is used for the point mass robot. This algorithm can be generalized for control of the unicycle mobile robot. For this aim, assuming that the output from the point mass robot is $u = (u_x, u_y)$, and the present location of the robot in the global coordinate system is $X = (x, y)$, the angular and linear velocity of the unicycle mobile robot obtained as below:

$$\theta_{Goal} = \arctan\left(\frac{u_y}{u_x}\right) \tag{39}$$

$$\omega = PID(\theta_{Goal} - \theta) \tag{40}$$

Using equation (22):

$$v = (\dot{x}^2 + \dot{y}^2)^{\frac{1}{2}} \Longrightarrow v = \|u\| = \left((u_x)^2 + \left(u_y\right)^2\right)^{\frac{1}{2}} \tag{41}$$

As shown in Fig. 11, in the FWS mobile robot, the linear velocity of the inside and outside wheels can be calculated using the linear velocity and angular velocity of the unicycle mobile robot.

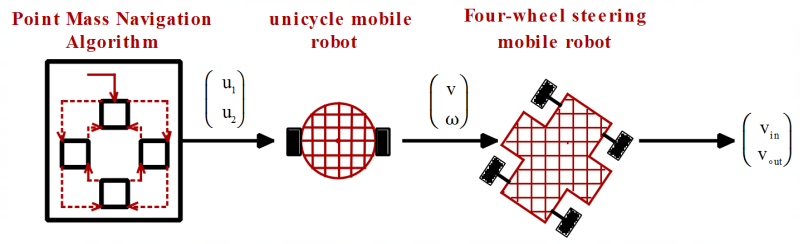

Figure 11. Planning model input to actual FWS mobile robot input.

4. Results and discussion

This section presents the results of the simulation tests that were performed on the FWS mobile robot to demonstrate the performance and effectiveness of the BBNA. This study uses the FWS mobile robot with the specifications outlined in Table 1[13].

Table 1. General specifications of the FWS mobile robot

Item	specification
Size	65.5×33.5 (L × W) cm
Max. Angular Velocity of Wheel's Steering	$0.74\ rad/sec$
Max. Linear Velocity of the Platform	$2.1\ m/s$
Radius of Wheels	$10\ cm$
Weight	$1177\ N$

Fig. 12, demonstrates how the FWS mobile robot moves using the BBNA strategy. As can be seen in the figure, some obstacles are in the way of the FWS mobile robot's progress towards the goal. With a BBNA, the robot travels the least amount of distance to reach its target. According to the trajectory of the CoG, there are two obstacles in the path of the robot. Therefore, using the introduced navigation algorithm, the robot will choose the appropriate behavior that allows the robot to will follow the wall around the obstacle clockwise or counterclockwise. Therefore, the

simulation results show that the BBNA can provide an optimal trajectory for the FWS mobile robot motion by timely switching between different behaviors.

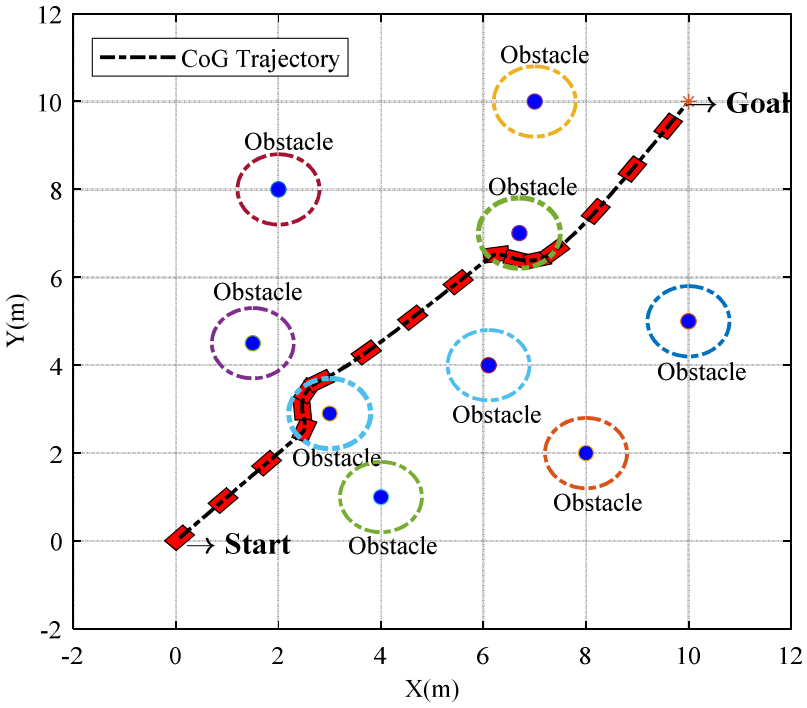

Figure 12. Robot trajectory with obstacle avoidance behavior.

As described in section 3, the commands of the BBNA are used for the point mass robot and we can use this algorithm for the unicycle mobile robot. The control input for X-direction and Y-direction of the point mass robot is depicted in Fig. 13. By applying the BBNA algorithm, the point mass robot model will be guided to the target position, and if there are obstacles in its path, the robot will follow the optimal path to avoid colliding with the obstacles, and follow the sidewall around each obstacle. The control commands represent the inputs of the robot speed control in the directions X and Y, so according to Fig. 13, based on the position of the robot and the obstacles, the amount of input speed to the robot will take both positive and negative values. If the robot follows the sidewall of an obstacle, the BBNA controller provides negative velocity values as input to X or Y direction, causing the robot to change its direction. As shown in this figure, since there were two obstacles along the trajectory of the point mass robot toward the goal, the control commands switched between GTG, $OA(FW_c)$ and $OA(FW_{cc})$. According to control inputs for point mass robot, the error function of X-direction and Y-direction is demonstrated in Fig. 14. As shown in this figure, when the robot starts moving towards the goal position, the error of X and Y direction is going to zero.

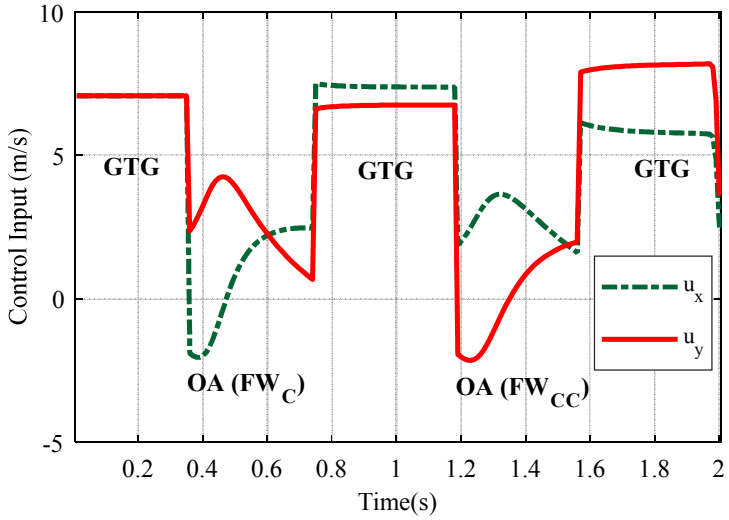

Figure 13. The control inputs to the point mass robot.

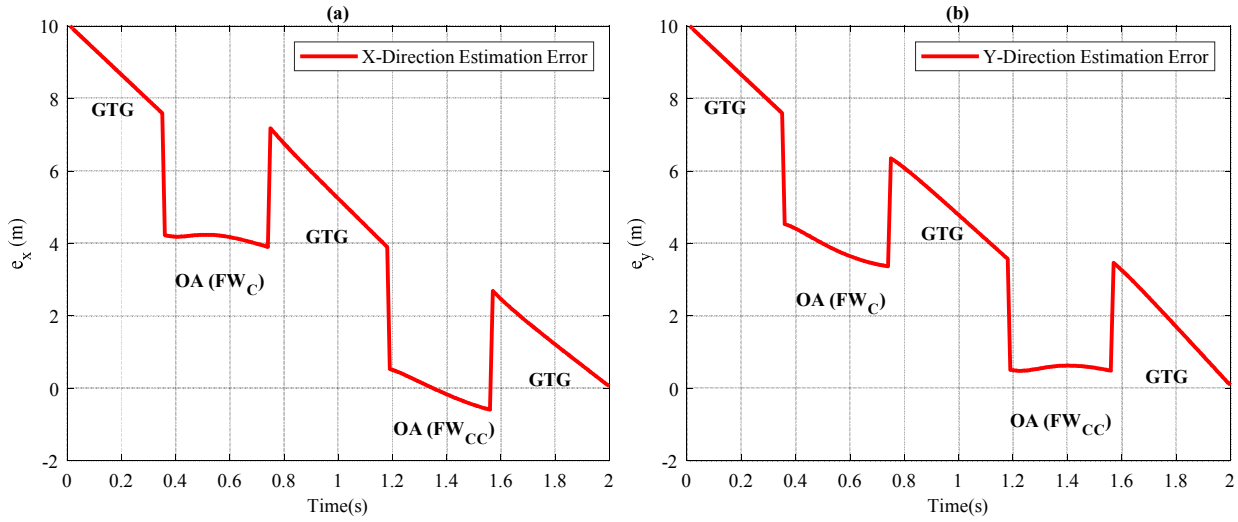

Figure 14. Estimation errors e_x and e_y for point mass robot.

As shown in Fig. 15, the linear velocity of the unicycle mobile robot can be calculated using equation (41) and the control commands from the point mass robot. One can observe, the linear velocity of the unicycle mobile robot is constant when it is performing the GTG behavior. However, when the robot is in OA behavior, the linear velocity is variable. It is worth mentioning that according to the dynamic equations obtained for the FWS mobile robot in section 2, the linear velocity of the unicycle mobile robot is equal to the linear velocity of the CoG of the FWS mobile robot.

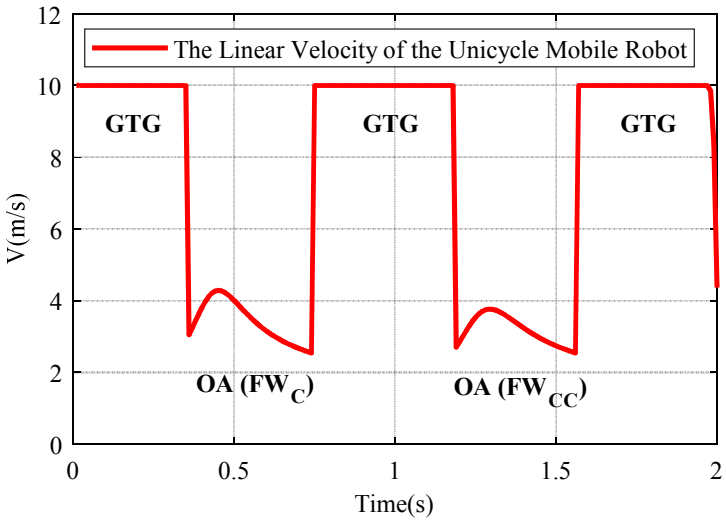

Figure 15. The linear velocity of the unicycle mobile robot

The angular velocity of the unicycle mobile robot is demonstrated in Fig.12. Since the FWS mobile robot and the unicycle mobile robot have the same dynamic equations, the angular velocity for both robots is the same. As shown in Fig. 16, the angular velocity of the robot is zero when the robot doesn't detect an obstacle in its path. However, the robot's angular velocity changes when it detects an obstacle in its path. Furthermore, the desired angle of the FWS mobile robot to achieve the goal is depicted in Fig. 17. As shown, before the robot reaching the obstacles, the desired angle of the robot is fixed and when the robot moving away from obstacles, the desired angle will change.

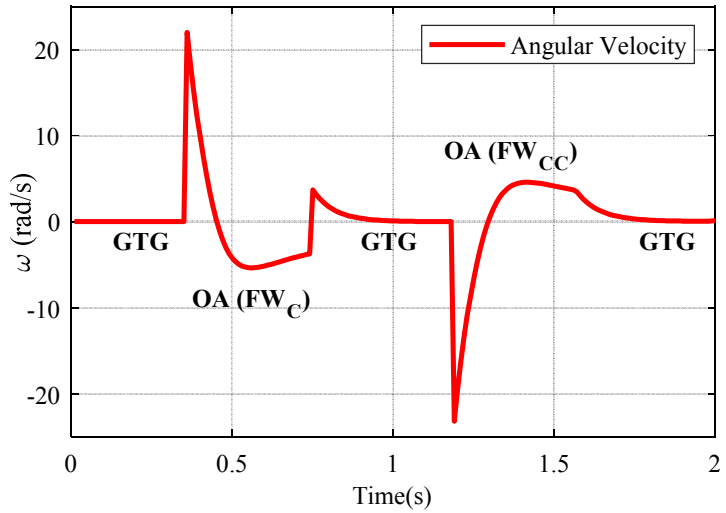

Figure 16. The angular velocity of the FWS mobile robot and unicycle mobile robot

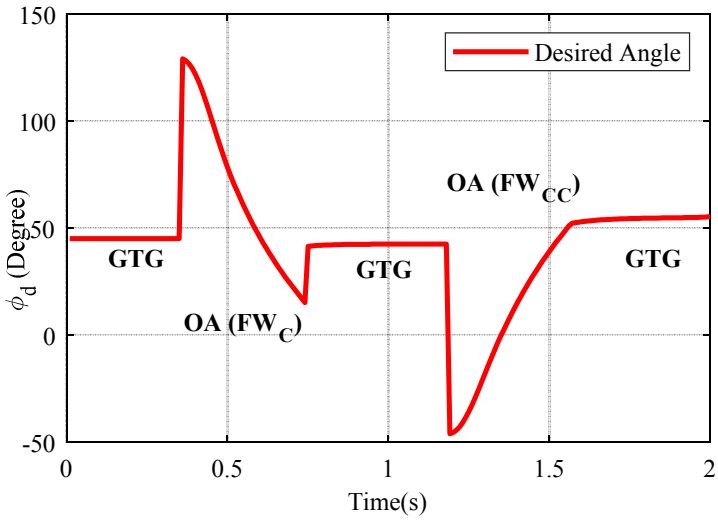

Figure 17. The desired angle of the FWS mobile robot to achieve the goal point

Fig. 18 shows FWS' inner and outer wheels' linear velocity. As can be observed, when the robot has a rectilinear motion to the goal, the linear velocity of the inside and outside wheels are the same, but in OA behavior, when the robot moving around obstacles, it has a curvilinear motion, therefore, the linear velocity of the inner and outer wheels is different.

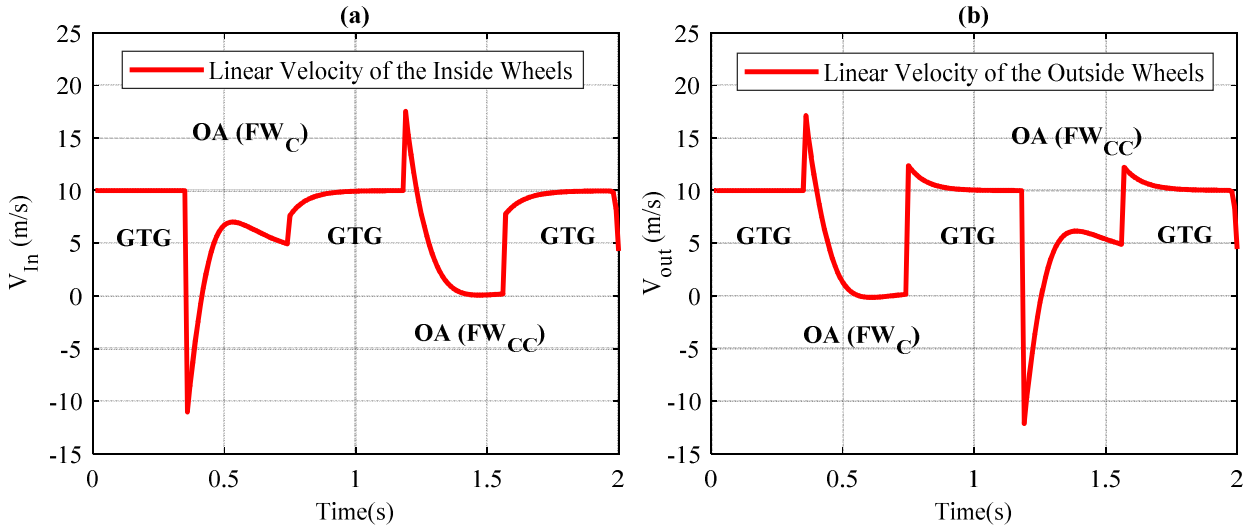

Figure 18. The linear velocity of the FWS mobile robot. a) Inside wheels b) Outside wheels.

The inside and outside wheels steering angles of the FWS mobile robot are affected by the length and width of the mobile robot. Fig. 19 illustrates how the width-length ratio affects steering angles of the inside and outside wheels of the FWS mobile robot. Whenever the width to length ratio of the robot is less than one, the robot appears thin. As the width increases and the length decreases, the robot will change from a thin appearance to a fat one. Fig. 19 shows that as the curvature radius increases, the rate of changing the steering angle for internal wheels of the lean robot is much lower than for external wheels. With increased width-to-length ratios of the FWS mobile robot, this situation will be reversed, such that the inner wheels will change steering angles at a higher rate than the outer wheels by increasing the radius of curvature. According to Fig. 19,

in a constant radius of curvature, the rate of change of steering angle for the inner wheels increases as the width to length ratio of the robot increases, whereas the opposite holds true for the outer wheels.

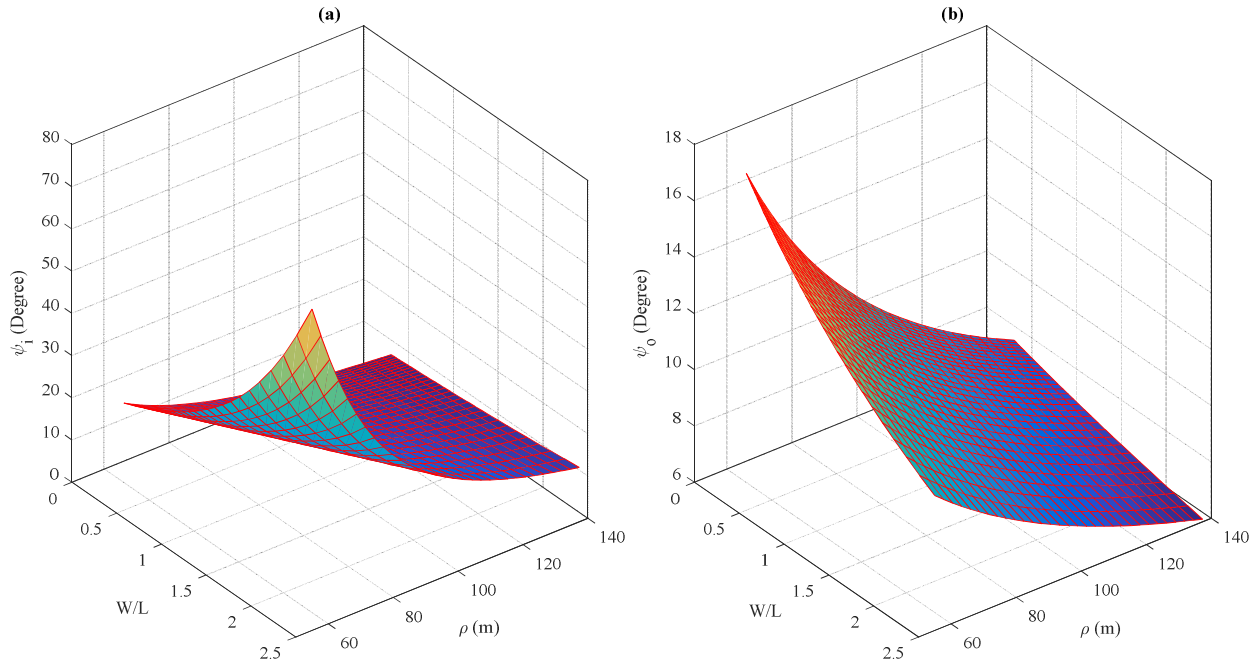

Figure 19. The effect of length and width of FWS mobile robot on the steering angle a) Inside wheels b) Outside wheels

5. Conclusion

This study focuses on the implementation of a behavior-based navigation algorithm (BBNA) on a four-wheel steering (FWS) mobile robot. It was shown that the proposed navigation algorithm consists of several nodes in which each node represents a different behavior of the mobile robot. The primary nodes of this algorithm were 'Go to Goal' and 'Obstacle Avoidance' so that switching between them was done by hard switches. In this control strategy, the transition between the primary nodes may occur more than once in a short period of time. This phenomenon is commonly known as Zeno, which is the cause of the chattering phenomenon that occurs in the control algorithm. In order to overcome this phenomenon, the navigation algorithm was strengthened by expanding the sliding dynamics between the 'Go to Goal' and 'Obstacle Avoidance' nodes on the switching surface. Added sliding nodes included moving around the boundary of the obstacles in clockwise and counterclockwise directions that caused the mobile robot to completely bypass obstacles. In addition, it was shown that the proposed algorithm is able to generate an optimal path to reach the goal point, depending on the robot's location, obstacles, and the goal. Since the BBNA is used for the point mass robot, therefore two transformations were used in order to transform the dynamic equations of the FWS mobile robot into a point mass robot. First, the mathematical models of FWS mobile robot dynamics were derived by using the Ackermann-Jeantnat model of steering, and then these dynamic model equations were converted into models of a unicycle mobile robot, and finally into models of a point mass. Based on the linear velocity of the center of gravity of the FWS mobile robot, the linear velocity of the inside and outside wheels of the robot was calculated. Results have shown that by using the BBNA, a FWS mobile robot can be a move toward

the goal without any collision with the obstacles. In addition, obtained results indicate that, when we have a thin FWS mobile robot in which the length of the robot is more than its the width, the radius of curvature increases, and consequently the rate of change of the steering angle of the inside wheels is lower than that of the steering angle of the outside wheels. On the other hand, if the ratio of width to length of the robot increases, the radius of curvature increases, and as the result, the rate of change of the steering angle of the inner wheels is more than that of the steering angle of the outer wheels.

6. References

1. Fuke, Y., Krotkov, E.: Dead reckoning for a lunar rover on uneven terrain. Proc. - IEEE Int. Conf. Robot. Autom. 1, 411–416 (1996). https://doi.org/10.1109/robot.1996.503811
2. Caracciolo, L., De Luca, A., Iannitti, S.: Trajectory tracking control of a four-wheel differentially driven mobile robot. Proc. - IEEE Int. Conf. Robot. Autom. 4, 2632–2638 (1999). https://doi.org/10.1109/robot.1999.773994
3. Roland Siegwart, Illah Nourbakhsh, D.S.: Introduction to Autonomous Mobile Robots - Roland Siegwart, Illah Reza Nourbakhsh, Davide Scaramuzza - Google Boeken. (2004)
4. Khadiv, M., Moosavian, S.A.A., Yousefi-Koma, A., Sadedel, M., Ehsani-Seresht, A., Mansouri, S.: Rigid vs compliant contact: an experimental study on biped walking. Multibody Syst. Dyn. 45, 379–401 (2019). https://doi.org/10.1007/s11044-018-09653-1
5. Sadedel, M., Yousefi-Koma, A., Khadiv, M., Mahdavian, M.: Adding low-cost passive toe joints to the feet structure of SURENA III humanoid robot. Robotica. 35, 2099–2121 (2017). https://doi.org/10.1017/S026357471600059X
6. Sadedel, M., Yousefikoma, A., Iranmanesh, F.: Analytical Dynamic Modelling of Heel-off and Toe-off Motions for a 2D Humanoid Robot. J. Comput. Appl. Mech. 46, 243–256 (2015). https://doi.org/10.22059/jcamech.2015.56215
7. Saenz, A., Santibañez, V., Bugarin, E., Dzul, A., Ríos, H., Villalobos-Chin, J.: Velocity Control of an Omnidirectional Wheeled Mobile Robot Using Computed Voltage Control with Visual Feedback: Experimental Results. Int. J. Control. Autom. Syst. 19, 1089–1102 (2021). https://doi.org/10.1007/s12555-019-1057-6
8. Nagatani, K., Noyori, T., Yoshida, K.: Development of multi-D.O.F. tracked vehicle to traverse weak slope and climb up rough slope. In: IEEE International Conference on Intelligent Robots and Systems. pp. 2849–2854 (2013)
9. Li, H., Zhao, Y., Lin, F., Zhu, M.: Nonlinear dynamics modeling and rollover control of an off-road vehicle with mechanical elastic wheel. J. Brazilian Soc. Mech. Sci. Eng. 40, 1–17 (2018). https://doi.org/10.1007/s40430-018-1009-8
10. Xu, X., Waters, T., Pickem, D., Glotfelter, P., Egerstedt, M., Tabuada, P., Grizzle, J.W., Ames, A.D.: Realizing simultaneous lane keeping and adaptive speed regulation on accessible mobile robot testbeds. 1st Annu. IEEE Conf. Control Technol. Appl. CCTA 2017. 2017-Janua, 1769–1775 (2017). https://doi.org/10.1109/CCTA.2017.8062713
11. Ajeil, F.H., Ibraheem, I.K., Azar, A.T., Humaidi, A.J.: Autonomous navigation and obstacle avoidance of an omnidirectional mobile robot using swarm optimization and sensors deployment. Int. J. Adv. Robot. Syst. 17, 172988142092949 (2020). https://doi.org/10.1177/1729881420929498
12. Oftadeh, R., Aref, M.M., Ghabcheloo, R., Mattila, J.: Bounded-velocity motion control of four wheel steered mobile robots. 2013 IEEE/ASME Int. Conf. Adv. Intell. Mechatronics Mechatronics Hum. Wellbeing, AIM 2013. 255–260 (2013).

https://doi.org/10.1109/AIM.2013.6584101
13. Oftadeh, R., Aref, M.M., Ghabcheloo, R., Mattila, J.: Mechatronic design of a four wheel steering mobile robot with fault-tolerant odometry feedback. IFAC (2013)
14. Sorour, M., Cherubini, A., Khelloufi, A., Passama, R., Fraisse, P.: Complementary-route based ICR control for steerable wheeled mobile robots. Rob. Auton. Syst. 118, 131–143 (2019). https://doi.org/10.1016/j.robot.2019.02.011
15. VertiGo wheeled robot isn't stopped by walls, https://newatlas.com/vertigo-wall-climbing-robot/41086/
16. Do, K.D.: Global inverse optimal exponential path-tracking control of mobile robots driven by Lévy processes. Robotica. 1–27 (2021). https://doi.org/10.1017/s0263574721000333
17. Valero, F., Rubio, F., Llopis-Albert, C.: Assessment of the Effect of Energy Consumption on Trajectory Improvement for a Car-like Robot. Robotica. 37, 1998–2009 (2019). https://doi.org/10.1017/S0263574719000407
18. Prasad, A., Sharma, B., Vanualailai, J.: A new stabilizing solution for motion planning and control of multiple robots. Robotica. 34, 1071–1089 (2016). https://doi.org/10.1017/S0263574714002070
19. Valera, Á., Valero, F., Vallés, M., Besa, A., Mata, V., Llopis-Albert, C.: Navigation of autonomous light vehicles using an optimal trajectory planning algorithm. Sustain. 13, 1–23 (2021). https://doi.org/10.3390/su13031233
20. Lee, J.K., Choi, Y.H., Park, J.B.: Sliding mode tracking control of mobile robots with approach angle in cartesian coordinates. Int. J. Control. Autom. Syst. 13, 718–724 (2015). https://doi.org/10.1007/s12555-014-0024-5
21. Fnadi, M., Menkouz, B., Plumet, F., Ben Amar, F.: Path Tracking Control for a Double Steering Off-Road Mobile Robot. In: CISM International Centre for Mechanical Sciences, Courses and Lectures. pp. 441–449 (2019)
22. Carlucho, I., De Paula, M., Acosta, G.G.: Double Q-PID algorithm for mobile robot control. Expert Syst. Appl. 137, 292–307 (2019). https://doi.org/10.1016/j.eswa.2019.06.066
23. Wang, D., Wei, W., Yeboah, Y., Li, Y., Gao, Y.: A Robust Model Predictive Control Strategy for Trajectory Tracking of Omni-directional Mobile Robots. J. Intell. Robot. Syst. Theory Appl. 98, 439–453 (2020). https://doi.org/10.1007/s10846-019-01083-1
24. Allagui, N.Y., Abid, D.B., Derbel, N.: Autonomous navigation of mobile robot with combined fractional order PI and fuzzy logic controllers. 16th Int. Multi-Conference Syst. Signals Devices, SSD 2019. 78–83 (2019). https://doi.org/10.1109/SSD.2019.8893176
25. Maalouf, E., Saad, M., Saliah, H.: A higher level path tracking controller for a four-wheel differentially steered mobile robot. Rob. Auton. Syst. 54, 23–33 (2006). https://doi.org/10.1016/j.robot.2005.10.001
26. Hu, C., Wang, R., Yan, F., Chen, N.: Output constraint control on path following of four-wheel independently actuated autonomous ground vehicles. IEEE Trans. Veh. Technol. 65, 4033–4043 (2016). https://doi.org/10.1109/TVT.2015.2472975
27. Wang, D., Qi, F.: Trajectory planning for a four-wheel-steering vehicle. In: Proceedings - IEEE International Conference on Robotics and Automation. pp. 3320–3325 (2001)
28. Caracciolo, L., De Luca, A., Iannitti, S.: Trajectory tracking control of a four-wheel differentially driven mobile robot. Proc. - IEEE Int. Conf. Robot. Autom. 4, 2632–2638 (1999). https://doi.org/10.1109/robot.1999.773994
29. Filipescu, A., Minzu, V., Filipescu, A., Minca, E.: Discrete-time sliding-mode control of a mobile platform with four driving/steering wheels. In: Lecture Notes in Electrical Engineering. pp. 401–409. Springer, Berlin, Heidelberg (2011)

30. Arkin, R., Arkin, R.: Behavior-based robotics. (1998)
31. Kortenkamp, D.Y., Bonasso, R.P., Murphy, R.: Artificial Intelligence and Mobile Robots. (1998)
32. Mahadevuni, A., Li, P.: Navigating mobile robots to target in near shortest time using reinforcement learning with spiking neural networks. Proc. Int. Jt. Conf. Neural Networks. 2017-May, 2243–2250 (2017). https://doi.org/10.1109/IJCNN.2017.7966127
33. M.Egerestedt: Control of Mobile Robots.
34. M. Egerstedt: Controls for the Masses. EEE Control Syst. Mag-azine. 33, 40–44 (2013)
35. Egerstedt, M.: Behavior based robotics using hybrid automata. Lect. Notes Comput. Sci. (including Subser. Lect. Notes Artif. Intell. Lect. Notes Bioinformatics). 1790, 103–116 (2000). https://doi.org/10.1007/3-540-46430-1_12
36. Khazaee, M., Sadedel, M., Davarpanah, A.: Behavior-Based Navigation of an Autonomous Hexapod Robot Using a Hybrid Automaton. J. Intell. Robot. Syst. Theory Appl. 102, (2021). https://doi.org/10.1007/s10846-021-01388-0
37. Armah: Implementation of Autonomous Navigation Algorithms on Two-Wheeled Ground Mobile Robot. Am. J. Eng. Appl. Sci. 7, 149–164 (2014). https://doi.org/10.3844/ajeassp.2014.149.164
38. Gautam, P., Sahai, S., Kelkar, S.S., Agrawal, P.S., D, M.R.: Designing Variable Ackerman Steering Geometry for Formula Student Race Car. Int. J. Anal. Exp. Finite Elem. Anal. 8, 1–11 (2021). https://doi.org/10.26706/ijaefea.1.8.20210101
39. Khan, A., Patel, M., Bhosale, O., Pawar, S., Patil, A.: A Review on Design and Assembly of Go- Kart Steering System. 193–197 (2021)
40. Hartani, K., Miloud, Y., Miloudi, A.: Electric Vehicle stability with rear Electronic differential Traction. Int. Symp. Enviroment Friendly Energies Electrcal Appllcations. 1–5 (2010)
41. Gillespie, T.D.: Fundamentals of Vehicle Dynamics. Fundam. Veh. Dyn. (1992). https://doi.org/10.4271/r-114
42. Hao, Y., Wang, J., Chepinskiy, S.A., Krasnov, A.J., Liu, S.: Backstepping based trajectory tracking control for a four-wheel mobile robot with differential-drive steering. Chinese Control Conf. CCC. 4918–4923 (2017). https://doi.org/10.23919/ChiCC.2017.8028131
43. Wu, X., Xu, M., Wang, L.: Differential Speed Steering Control for Four-Wheel Independent Driving Electric Vehicle. Int. J. Mater. Mech. Manuf. 355–359 (2013). https://doi.org/10.7763/ijmmm.2013.v1.77